ELSEVIER

Journal of Nuclear Materials 313–316 (2003) 327–332

journal of nuclear materials

www.elsevier.com/locate/jnucmat

Erosion and migration of tungsten employed at the main chamber first wall of ASDEX Upgrade

K. Krieger [a,*], A. Geier [a], X. Gong [b], H. Maier [a], R. Neu [a], V. Rohde [a], ASDEX Upgrade Team

[a] *Max-Planck-Institut für Plasmaphysik, IPP-EURATOM Association, 85748 Garching, Germany*
[b] *Institute of Plasma Physics, Academia Sinica, Hefei, Anhui 230031, China*

Abstract

In ASDEX Upgrade, tungsten is employed as plasma facing material at the central column of the plasma main chamber. The campaign averaged tungsten erosion flux was determined by measuring the difference of the W-layer thickness before and after experimental campaigns using ion beam analysis methods. The lateral variations of the observed tungsten erosion flux reflects the pattern of magnetic field lines intersecting the respective plasma facing surfaces. Long term migration and redeposition of eroded tungsten were investigated by ion beam analysis of deposited tungsten on wall samples from main chamber and divertor. The obtained results, as well as the spectroscopically observed low tungsten plasma penetration probability, indicate that a major fraction of the eroded tungsten migrates predominantly through direct transport channels in the outer plasma scrape-off layer without entering the confined plasma.

PACS: 52.40.H; 52.25.V
Keywords: Tungsten; Erosion; Redeposition; Impurity transport; Tokamak; Plasma facing material

1. Introduction

Tungsten has been used as plasma facing material for increasingly larger fractions of the 8.2 m^2 inner column first wall of ASDEX Upgrade. It is a promising alternative to low-Z materials such as carbon and beryllium, primarily because of its high sputtering threshold energy [1] and its low sputtering yield. One has, however, to ensure that the W plasma concentration stays below a limit of approximately 2×10^{-5} for ignited fusion plasmas [2] to avoid excessive energy losses due to the strong specific line radiation power of tungsten [3] in the respective temperature range. Corresponding limits for low-Z materials are of the order of 1% [2]. Spectroscopic measurements of the tungsten plasma concentration demonstrate that the concentration limit can be met for all fusion reactor relevant discharge scenarios [4–6]. Apart from the tungsten plasma concentration, W erosion and migration processes impose further boundary conditions on the suitability of tungsten as first wall material. Since the W erosion and deposition fluxes are generally too small for spectroscopic detection [6], these processes were mainly studied by post campaign ex-situ analysis of wall samples using ion beam methods.

2. Experimental setup

To minimize the risk of adverse effects on plasma performance by possible excessive tungsten influx, the W covered area at the inner column was increased in several steps during three subsequent experimental campaigns from 1999–2002 as shown in Fig. 1. In W campaign phase I (1999/2000) two toroidal rows of W coated graphite tiles were installed at the lower edge of the central column covering an area of 1.3 m^2. During phase I the tiles were exposed to 919 discharges with an

* Corresponding author. Tel.: +49-89 32 99 1655; fax: +49-89 32 99 2279.
E-mail address: krieger@ipp.mpg.de (K. Krieger).

0022-3115/03/$ - see front matter
PII: S0022-3115(02)01351-X

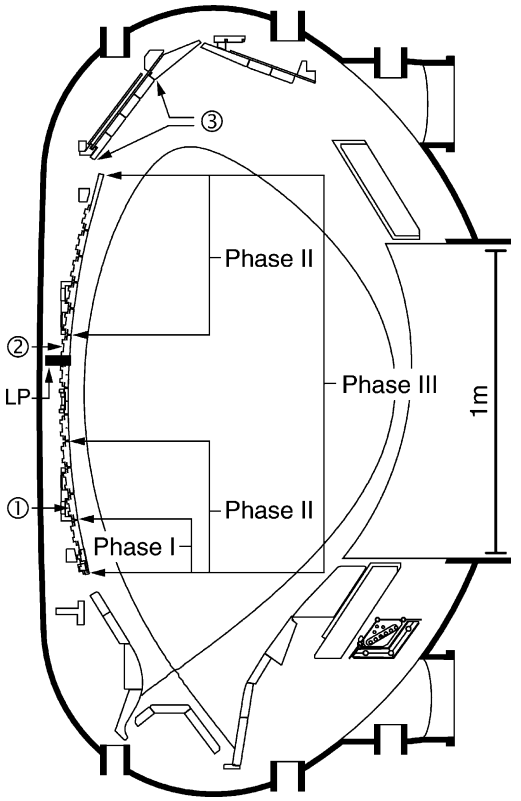

Fig. 1. Poloidal cross-section of the ASDEX Upgrade vessel with W-coated areas for the first three phases of tungsten usage at the central column. Positions 1, 2 and 3 denote tile positions referenced in the section on W redeposition. LP denotes the position of a Langmuir probe commissioned in phase III.

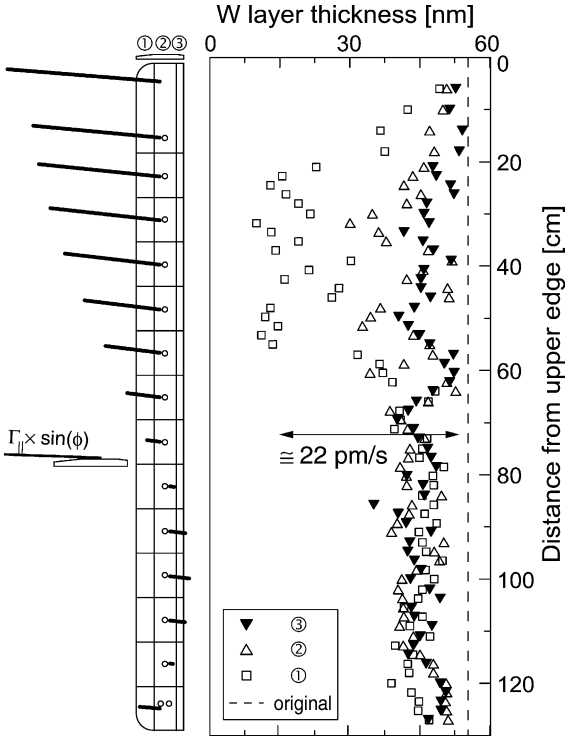

Fig. 2. Erosion of the tungsten coating along a complete vertical column of heat shield tiles employed during phase II. The poloidal coordinate denotes the distance along the tile surfaces from the top edge of the heat shield. Post campaign layer thickness was measured at three facettes of the tiles. The schematic view of the tile column shows the local pitch angle of magnetic field lines intersecting the tile surfaces. The length of the respective line segments corresponds to the fraction $\Gamma_{\|} \times \sin(\phi)$ of the parallel ion flux reaching the surface, where ϕ denotes the field line angle of incidence against the tile surface.

accumulated discharge time of 4600 s. In the subsequent W phase II (2001) with 374 discharges and 1780 s accumulated plasma exposure time the tungsten coated area was extended to two belts of tiles with a total area of 5.5 m^2. In addition, two columns of W coated tiles were installed covering the full poloidal extent of the heat shield to allow analysis of the spatial distribution of the W erosion also in the midplane limiter region. For one of the W tile columns the thickness of the coating was reduced to 60 nm to increase the sensitivity of erosion measurements. To achieve a closed W-layer, the surface of the respective tiles was additionally polished. Uniformity of surface coverage and layer thickness were confirmed by scanning electron microscopy [7]. Details on the manufacturing, pre- and post-fabrication tests and on the properties of the coatings can also be found in [7].

In the most recent W phase III with 623 discharges and 3690 s accumulated plasma exposure time as of March 2002, W coverage was finally extended to the midplane region of the central column. This area is used as limiter during plasma ramp-up and ramp-down and therefore subject to the highest plasma flux and heat loads. The W coated area was increased to 7.1 m^2 with carbon fibre composite tiles left in two areas facing neutral beam injection shine through. To reduce excessive erosion at leading edges, the tiles were shaped trapezoidally (cross-section shown in Fig. 2) and mounted in pairs facing opposite toroidal direction.

In the W campaign phases I–III the plasma was mainly operated in H-mode (63% of all discharges) with typical edge densities of the order 10^{19} m^{-3} and edge temperatures of $\approx$100 eV, decreasing to $\approx$10 eV in the scrape off layer [8].

3. Tungsten erosion

Tungsten erosion was studied by ex-situ ion beam analysis of the W-coated tiles using Rutherford backscattering analysis (RBS) [9]. After W phase II, the complete vertical column of 14 W-coated tiles with 60 nm

coating thickness was removed to determine the poloidal variation of the W erosion flux. Fig. 2 shows the remaining layer thickness along the poloidal distance from the upper edge of tile 1 at the top of the inner column plotted for the three different facets of the tiles. The difference to the thickness of the virgin layer reflects the campaign integral of the W net erosion flux. The maximum W-erosion is found at tile facet 1 of rows 2–6. The corresponding campaign averaged erosion flux is derived by dividing the area density of eroded W by the total plasma exposure time. One obtains a maximum W erosion rate of 22 pm/s, which is quite similar to the erosion rate of 17 pm/s measured at the lowest tile row 14 in the previous campaign phase I [10]. Towards the lower half of the central column the erosion rate at facet 1 decreases steeply to a base level of ≈5 pm/s. Similar rates are found at tile facets 2 and 3 with an increase to ≈10 pm/s for the tangential tile facet 2 at rows 2–6 similar to the spatial distribution at facet 1.

From the spatial variation and the magnitude of the tungsten erosion flux, impact of ions has been identified as the predominant erosion channel [9,11]. Taking this into account, the observed spatial distribution of the erosion rate can be understood as a result of the intersection pattern of the magnetic field lines with the tile surfaces. For a given surface location the angle of incidence ϕ can be calculated from the scalar product $\vec{N} \cdot \vec{B}$ of the normalized surface vector $\vec{N}$ and the local magnetic field $\vec{B}$. The magnetic field can be derived from the reconstructed magnetic equilibriae [12]. Fig. 2 shows the resulting pattern for the flat top phase of a typical H-mode discharge with low triangularity shaping. The length of the line segments corresponds to the fraction $\Gamma_{\parallel} \times \sin\phi$ of the parallel ion flux reaching the surface. Since there are no experimental data for the absolute local values of $\Gamma_{\parallel}$, the line segments provide, however, only an estimate for the relative spatial distribution of the incident flux. With typical values of $\phi < 2°$ at tangential surfaces, the incident flux at toroidally inclined tile surfaces will be either shadowed or elevated depending on the orientation against the incident B field and on the shape and distance of the preceding upstream tile.

At the upper half of the central column, the field line angle of incidence is significantly higher than that for the lower half. Therefore the incident ion flux is higher at the upper half leading to increased erosion. This effect can be further enhanced because field lines intersecting the central column above the midplane are usually connected to the outer midplane region, while field lines intersecting tiles below the midplane are connected to the inner divertor. This might lead to a correspondingly higher ion flux from corresponding flux tubes compared to flux tubes to the inner divertor at the same flux surface with a much smaller connection length.

The field line intersection pattern also explains the maximum erosion at facet 1 of tile rows 2–6. Since the incident field lines come from left, their angle of incidence at facet 1 is increased over the tangential facet 2, leading to significantly elevated ion fluxes and correspondingly increased erosion rates. In contrast, at the lower half of the central column, facet 1 is shaded from the magnetic field lines incident from the right side.

In addition to the geometric effects, the radial variation of the plasma parameters needs to be considered for a complete interpretation of the observed poloidal erosion pattern. Field lines belonging to flux surfaces farther away from the separatrix will carry a smaller ion flux with lower ion temperature. In Fig. 2 the corresponding poloidal flux of the B field lines at the tile surfaces increases towards the top of the inner column. The radial decrease of ion temperature and that of parallel ion flux explains the corresponding steep decrease of the erosion rate towards the upper edge despite the comparatively high angle of incidence.

The discussed erosion model is further supported by time resolved measurements of the local plasma temperature and density at the central column. A Langmuir probe was installed near the midplane of the central column at the location shown in Fig. 1. The time evolution of the local plasma temperature and density recorded by this probe during a typical H-mode discharge is shown in Fig. 3(b). During plasma ramp up and ramp down phases, the electron density is increased by up to two orders of magnitude over the value during the flat-top phase, while the electron temperature decreases by a factor of ≈3 due to the lower heating power. Apart from the closer proximity of the separatrix to the tiles just above the vessel midplane, the field line inclination angles in this region are increased over the values during the plasma flat-top due to the circular plasma shape used in ramp-up and ramp-down phases. The combination of both effects explains the strongly elevated ion flux during these discharge phases. This should lead to significant contributions of these phases to the observed campaign integrated W-erosion. Spectroscopic observation of a neutral tungsten emission line at the central column [6] allowed to determine the W gross erosion flux for a

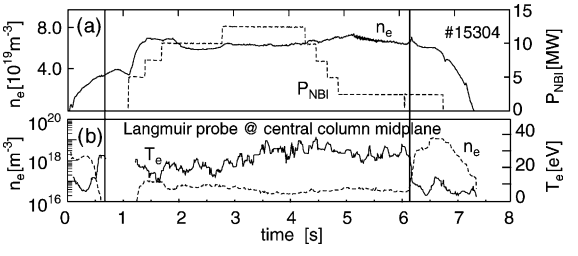

Fig. 3. Time evolution of local electron density and temperature at the midplane position of the central column in a H-mode discharge (b). The traces in (a) represent line averaged electron density and neutral beam heating power.

number of discharges. In ramp down phases with additional neutral beam heating W erosion rates of up to 50 pm/s were observed above the central column midplane whereas during flat top phases the W I line emission was below the detection limit [6]. Using these data, the campaign integral of the W gross erosion in ramp down phases was estimated by assuming similar erosion fluxes in all discharges. This results in a contribution of approximately 30% to the measured erosion of the W-layer. This fraction is, however, only an upper limit because the spectroscopic measurements reflect W gross erosion whereas the measured erosion of the W layer represents net erosion.

Since the sputtering threshold energy of deuterium ions incident on tungsten is 201 eV [1], the measured temperature range finally proves that the observed W erosion must be attributed to impact of impurity ions. The main impurity in ASDEX Upgrade is carbon with typical fractions in the 1% range, which is sufficient to explain the measured W erosion as already observed in the tungsten divertor campaign [13].

4. Tungsten migration and redeposition

Migration and redeposition of eroded tungsten were investigated by post-campaign analysis of tungsten deposition on carbon tiles from central column and divertor. In first measurements RBS with 1.5 and 3.0 MeV protons was used [9]. With the recent availability of a new detector type the sensitivity for tungsten, particularly in deposition dominated areas could be greatly increased by using proton induced X-ray emission (PIXE) analysis. Fig. 4 shows the W redeposition rate for two graphite tiles removed from the inner column at position 1 and 2 in Fig. 1 after W phase I. The tile at position 1 directly above the W coated tile rows shows a steep, approximately exponential, decrease of the redeposition rate with increasing poloidal distance to the tungsten coating and a decay length of $\approx$3.5 cm. The redepositon rate on the tile at position 2 near the midplane of the central column is an order of magnitude smaller, similar to values found at the inner upper divertor plate (position 3 in Fig. 1). The pattern at the tile directly above the tungsten coated rows can be explained by the direct connection along magnetic field lines between the plasma layer in front of the tungsten coated tiles and the graphite tiles above. A part of the eroded tungsten will directly migrate to the graphite tiles along the magnetic field after ionisation. The strong variation of the W deposition rate in toroidal direction is due to shading of field lines by the toroidally adjacent upstream tile similar to the effect observed in the erosion measurements.

Fig. 5 shows the tungsten deposition rate along the poloidal extension of the respective baffle and divertor

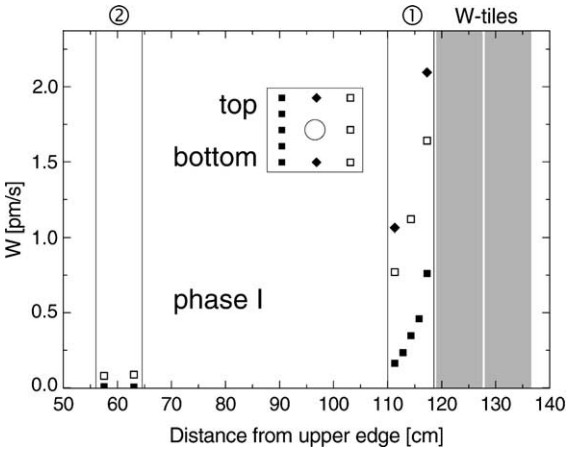

Fig. 4. Tungsten redeposition rate during W campaign phase I at two graphite tiles, directly above the tungsten coated area and at the central column midplane position as shown in Fig. 1.

tiles removed after phase I. The maximum tungsten deposition rate is found at the edge of the inboard horizontal closure tiles, with a steep decrease at increasing radial distance from the plasma and also strongly decreasing towards the vertical baffle module. This can be explained by field line tracing calculations, which show that for typical plasma configurations there is a direct connection along magnetic field lines between the two tile rows at the lower edge and the horizontal closure tiles.

The W deposition rates at the baffle modules are quite similar at inner and outer divertor throat. At the strike point zones, where the W deposition was below the detection limit for RBS, the PIXE results revealed a deposition rate more than two times the value at the

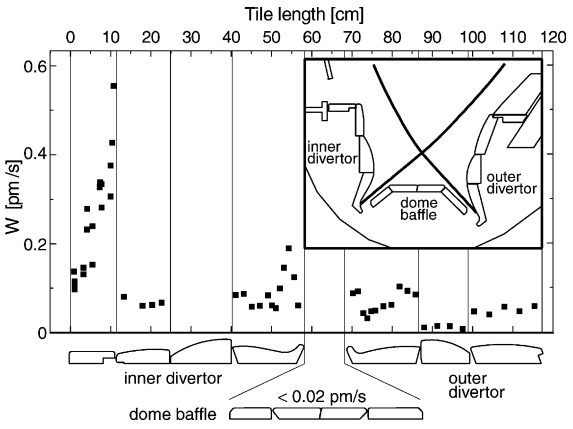

Fig. 5. Tungsten redeposition rate in the divertor during the W phase I campaign with divertor II configuration. The inset shows a poloidal cross-section of the divertor area. The deposition rate is plotted along the poloidal length of the respective baffle and divertor tiles.

baffle tiles. The reason for the weak sensitivity of RBS is the great depth range over which the tungsten is spread out in deposited carbon layers.

Beginning with W phase II the divertor configuration IIb was used, to allow plasma shapes with higher triangularity. Fig. 6 shows the tungsten deposition rate along the poloidal extension of the respective baffle tiles removed after W phase II and during a maintenance vent in phase III respectively. As in divertor II configuration the deposition rates at the inner divertor baffle increase towards the areas closer to the separatrix decreasing again along the vertical part of the baffle towards the strike point zone. The inner baffle tiles removed after W phase II show similar deposition rates as in W phase I despite the much larger W coated area. This indicates that the area of the central column directly connected to the divertor throat is similar in both configurations. On the inner baffle tiles removed in W phase III, the W redeposition rate is, however, approximately two times larger, presumably to the additional source of tungsten from the midplane area, which is generally closest to the separatrix.

The high W deposition rate at surfaces, which are in contact only with the outer low density region of the edge plasma, indicates that a major fraction of the eroded tungsten migrates directly through the plasma scrape-off layer without entering the confined plasma. While slightly increased W deposition rates are also observed in the strike point region of inner and outer divertor, this must be seen in relation to the incident plasma flux, which is 1–2 orders of magnitude higher than ion fluxes at tiles in contact with the far edge plasma. The dominance of W migration paths in the edge plasma can be explained by the comparatively short ionisation length of eroded tungsten atoms, which leads to a good shielding by the edge plasma and is in agreement with spectroscopic measurements of a W-penetration probability in the range of 1% [4] as well as with recent tungsten transport modeling using the DIVIMP code [14].

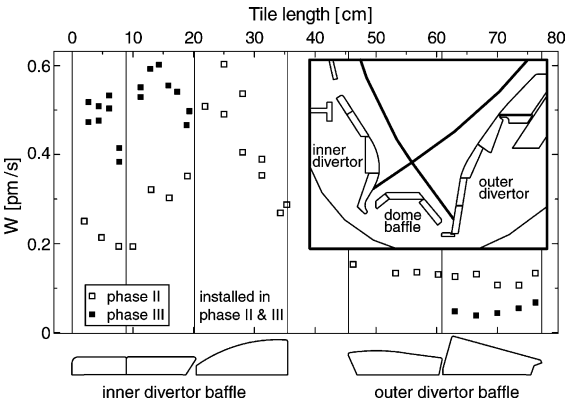

Fig. 6. Tungsten redeposition rate at the divertor baffle during the W phase II and phase III campaigns with divertor IIb configuration. The inset shows a poloidal cross-section of the divertor area. The deposition rate is plotted along the poloidal length of the respective baffle tiles.

Comparison of the integral W erosion with the deposition rates in the divertor shows that only about 10% of the eroded tungsten migrates to the divertor. This can be explained partly by the effects of prompt redeposition and local redistribution at the heat shield as discussed above. In addition, erosion from plasma ramp-up and ramp-down with circular plasmas will not contribute to W divertor deposition.

5. Summary

In subsequent experimental campaigns ASDEX Upgrade has been operated with large area tungsten plasma facing components in the main chamber. Tungsten coated graphite tiles were introduced at the central column heat shield with the area increased up to almost complete coverage.

The spatial distribution of the W erosion rate can be explained by the geometric pattern of magnetic field lines intersecting plasma facing surfaces. As a consequence, circular plasma cross sections lead to increased W erosion, which is particularly important for plasma ramp-up and ramp-down phases. The erosion rate might be further reduced by appropriate shaping of plasma facing surfaces, however, the gain will be limited by the mounting accuracy of the components.

The maximum average W erosion rate was found to be $\approx$20 pm/s as compared to the predicted value of 0.6–3 pm/s for the ITER design (50 pm/s for Be) [15].

Tungsten redeposition rates are maximal at surfaces in contact with outer edge plasma regions. This observation and the low tungsten plasma penetration probability demonstrate the good shielding of eroded tungsten from the confined plasma and the prevalence of direct migration channels in the edge plasma over transport through the confined plasma region. Consequently, tungsten plasma concentrations in fusion relevant discharge scenarios have as yet remained far below the maximum tolerable limit despite the increased tungsten source term.

References

[1] W. Eckstein, C. García-Rosales, J. Roth, W. Ottenberger, Sputtering data, IPP Report, IPP 9/82, 1993, p. 337.
[2] N. Peacock, R. Barnsley, N. Hawkes, K. Lawson, M. O'Mullane, in: P. Stott, G. Gorini, E. Sidoni (Eds.), Diagnostics for Experimental Thermonuclear Fusion Reactors, Varenna (Italy), Plenum, New York, 1996, p. 291.
[3] D. Post, R. Jensen, C. Tarter, et al., At. Data Nucl. Data Tables 20 (1977) 397.

[4] R. Neu, R. Dux, A. Geier, A. Kallenbach, R. Pugno, V. Rohde, et al., Plasma Phys. Contr. Fus. 44 (2002) 811.
[5] R. Neu, V. Rohde, A. Geier, K. Krieger, H. Maier, et al., J. Nucl. Mater. 290–293 (2001) 206.
[6] R. Neu et al, New Results of the Tungsten Programme in ASDEX Upgrade, these Proceedings, I08.
[7] H. Maier, J. Luthin, M. Balden, J. Linke, F. Koch, H. Bolt, Surf. Coat. Technol. 142–144 (2001) 733.
[8] J. Neuhauser, D. Coster, H.U. Fahrbach, J.C. Fuchs, G. Haas, A. Herrmann, et al., Plasma Phys. Control. Fus. 44 (2002) 855.
[9] K. Krieger et al., Erosion and migration of tungsten employed at the central column heat shield of ASDEX Upgrade, ICFRM-10, 2001, J. Nucl. Mater., in press.
[10] W. Schneider, D. Hildebrandt, K. Krieger, R. Neu, V. Rohde, J. Roth, et al., in: Europhysics Conference Abstracts (CD-ROM), Proceedings of the 28th EPS Conference on Controlled Fusion and Plasma Physics, Madeira, 2001, p. 1044.
[11] G. Tabasso, H. Maier, et al., Nucl. Fus. 40 (2000) 1441.
[12] P.J. McCarthy, P. Martin, W. Schneider, The CLISTE Interpretive Equilibrium Code, IPP Report 5/85, 1999.
[13] K. Krieger, H. Maier, R. Neu, J. Nucl. Mater. 266–269 (1999) 207.
[14] A. Geier et al., Modeling of tungsten transport in the SOL for sources at the central column of ASDEX Upgrade using DIVIMP, these Proceedings, p. 3.68.
[15] G. Janeschitz et al., J. Nucl. Mater. 290–293 (2001) 1.